1   **mTOR S-nitrosylation inhibits autophagy and lysosomal proteolysis**

2   Bryce W.Q. Tan[1,2], Sijie Tan[3], Byorn W.L. Tan[4], Sheeja Navakkode[1], Cheng Yang Ng[5],

3   Steven Yuan[5], Mui Cheng Liang[1], Chao Liu[1,6,7], Shi Yin[1], Chou Chai[1], Katherine C.M.

4   Chew[1], Yee Kit Tai[1], Sreedharan Sajikumar[1], Yulin Lam[5], Ping Liao[4], Han-Ming Shen[1], Kah-

5   Leong Lim[1], Esther Wong[1,3,8], Tuck Wah Soong*[1,4,9,10]

6   **Affiliations**

7   [1]Department of Physiology, National University of Singapore, Singapore 117593

8   [2]Department of Medicine, National University Health System, Singapore

9   [3]School of Biological Sciences, Nanyang Technological University, Singapore 637551

10   [4]National Neuroscience Institute, Singapore 308433

11   [5]Department of Chemistry, National University of Singapore, 3 Science Drive 3, Singapore

12   117543

13   [6]Jiangsu Province Key Laboratory of Anesthesiology

14   [7]Jiangsu Province Key Laboratory of Anesthesia and Analgesia Application Technology,

15   Xuzhou Medical University, Xuzhou, China

16   [8]Centre for Healthy Ageing, National University Health System, Singapore 117456

17   [9]LSI Neurobiology Programme & MSC Neuroscience Programme, National University of

18   Singapore 117456

19   [10]NUS Graduate School for Integrative Sciences and Engineering, National University of

20   Singapore 117456

21   **Corresponding Author:** Prof Soong Tuck Wah, Department of Physiology, National

22   University of Singapore, Singapore, email: phsstw@nus.edu.sg

23 **Abstract**

24 Mammalian Target of Rapamycin (mTOR) is a master regulator of autophagy and lysosomes,

25 and its downstream kinase-dependent pathways have been extensively characterized. Here,

26 we report an unexpected kinase-independent regulation of autophagy and lysosomes by S-

27 nitrosylation at Cys423 position of mTOR that resulted in suppression of VPS34 and

28 PIKfyve-dependent phosphoinositide synthesis. Physiologically, S-nitrosylation of mTOR

29 reduced basal lysosomal proteolysis via nitric oxide synthase (NOS)-mediated synthesis of

30 NO from lysosomal arginine precursor, a marker of cellular nutrition status. Significantly, we

31 found increased lysosomal NOS-mTOR complexes in APP-PS1 Alzheimer's disease (AD)

32 murine model, and increased mTOR S-nitrosylation in AD patient-derived fibroblasts. Lastly,

33 we demonstrated that pharmacological inhibition of NOS or overexpression of mTOR^{Cys423Ala}

34 mutant reversed lysosomal and autophagic dysfunction in AD patient-derived fibroblasts,

35 suggesting novel therapeutic strategies for autophagosome-lysosomal activation.

36 **Keywords:** Nitric oxide synthase, nitrosylation, mTOR, autophagy, lysosomes,

37 phosphoinositide, Alzheimer's Disease

Introduction

S-nitrosylation of proteins, including XIAP(*1*) and PDI(*2*), plays a critical role in neurodegeneration(*3, 4*). While recent evidences suggest that arginine is a critical amino acid in mTOR regulation of lysosomal activity(*5, 6*), the pathophysiological relevance of lysosomal arginine is not well understood. Emerging studies have implicated aberrant S-nitrosylation(*7, 8*) and dysfunctional arginine metabolism(*9, 10*) in Alzheimer's Disease(AD) where autophagosome-lysosomal failure contribute to tau and amyloid burden(*11-13*). Taken together, these studies suggest a possible pathophysiological link between arginine, nitrosative stress and autophagosome-lysosomal failure. As arginine is important for nitric oxide synthesis, and the physiological role of lysosomal nitric oxide synthase (NOS) is poorly understood(*14*), we hypothesize that lysosomal arginine, under nutrient-replete conditions, serves as a critical substrate of lysosomal NOS that mediate mTOR S-nitrosylation. This physiological cellular mechanism to sense lysosomal arginine stores will lead to appropriate downstream inhibition of autophagy, while excessive mTOR S-nitrosylation under pathophysiological conditions such as AD contribute towards autophagosome-lysosomal dysfunction.

Results

NO mediates autolysosome dysfunction

To determine the effect of NO on autophagy and lysosome function, HEK 293 cells treated with low-dose (4 µM) long-lived NO donor NOC18 have reduced number of autolysosomes (**Figure 1A-B**), and accumulation of perinuclear lysosomes as detected by lysomotropic dye Lysotracker Red and GFP-LAMP1 puncta (**Figure 1C-D**), with decreased lysosomal Cathepsin B proteolysis activity(**Figure 1E-F**). We next investigated effects of NOC18 on other endosomal compartments and did not observe any significant difference in numbers of

63 early endosomes (EEA1-positive; **Figure 1G**), pre-autophagosomes(ATG16L1-positive;

64 **Figure 1H**), or late endosomes (Rab7A-positive; **Figure 1I-J**). Following, we examined if

65 the observed autophagic and lysosomal deficits could be explained by transcriptional

66 dysregulation, and found no alterations in nuclear translocation or phosphorylation of

67 transcriptional factor TFEB (**Figure 1-figure supplement 1 A-D**). By contrast, we found

68 marked TFEB nuclear translocation with high-dose NOC18(500 μM), as was reported by

69 others(*15*). In view of concomitant lysosomal and autophagic deficits with NOC18, we

70 wondered if S-nitrosylation of mTOR, a major signalling regulator of the autophagosome-

71 lysosomal pathway, could be a possible underlying mechanism. Significantly, mTOR was S-

72 nitrosylated, but none of its phosphorylated forms (S2448 or S2481) could be detected,

73 suggesting that only non-phosphorylated forms can be S-nitrosylated (**Figure 1K**).

74 Intriguingly, we observed that mTOR and its substrate p70S6K, ULK1, and AKT

75 phosphorylation levels were not altered with NOC18 (**Figure 1L-O; Figure 1-figure**

76 **supplement 1 E-G**). In contrast, treatment of Torin-1 reversed NOC18-mediated lysosomal

77 accumulation (**Figure 1-figure supplement 1 H**), impairment of lysosomal proteolysis and

78 autophagy (**Figure 1-figure supplement 1 I-J),** suggesting kinase-independent effects of S-

79 nitrosylated mTOR. This corroborates with initial observations that only non-phosphorylated

80 forms of mTOR could be S-nitrosylated. As VPS34 and PIKfyve are two major kinases

81 regulating autophagy and lysosomal activity, we next hypothesized if mTOR functionally

82 regulate these kinases in NOC18-treated cells. Of note, there were increased mTOR-VPS34

83 and mTOR-PIKfyve interactions in NOC18-treated cells (**Figure 1P**) that were rapamycin-

84 insensitive(**Figure 1Q**), while no significant increase in Rictor or Raptor binding with mTOR

85 was observed with NOC18 treatment(**Figure 1P**). These evidences are in keeping with the

86 kinase-independent effects of S-nitrosylated mTOR. Finally, we found that phosphoinositide

87 species PI(3)P and PI(3,5)P$_2$, products of VPS34 and PIKfyve respectively, were both

88   downregulated in NOC18-treated cells(**Figure 1R**), which is in keeping with previous studies

89   on the regulatory role of mTOR on these kinases(*16, 17*).
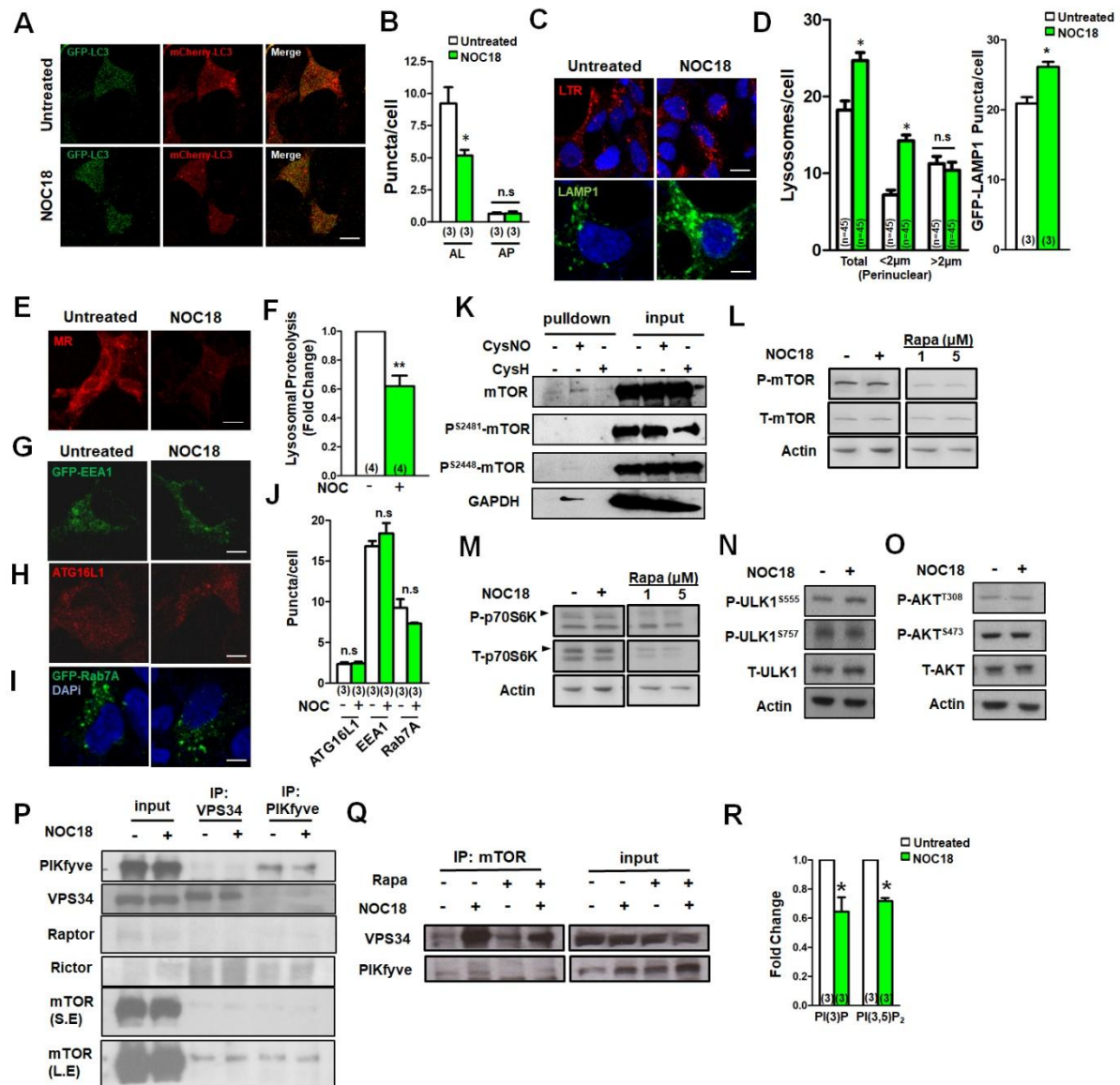
90   **Figure 1**

91

92

93   **Figure 1: S-nitrosylation of mTOR is kinase-independent.** (**A**)mCherry-GFP-LC3-

94   transfected HEK293 cells treated with NOC18 and (**B**)quantification of autolysosomes (AL)

95   and autophagosomes (AP). (**C**)Lysotracker staining and GFP-LAMP1 overexpression of

96   NOC18-treated HEK293 cells and (**D**)quantification of lysosomal distribution and GFP-

97   LAMP1 puncta. **(E)**Magic Red Cathepsin-B substrate staining of NOC18-treated cells and

98   **(F)**quantification graph. **(G)**GFP-EEA1-, **(H)**mCherry-ATG16L1-, and **(I)**GFP-Rab7A

99   transfected HEK293 cells and **(J)**puncta quantification. **(K)**Resin-assisted capture of mTOR

100   and GAPDH. Immunoblot of **(L)**phosphorylated mTOR, **(M)**p70S6K, **(N)**ULK1 and

101   **(O)**AKT. **(P)** VPS34 and PIKfyve immunoprecipitation, and detection of mTOR, Rictor and

102   Raptor(S.E. – short exposure for input; L.E.–long exposure for immunoprecipitated VPS34

103   and PIKfyve) **(Q)** mTOR immunoprecipitation and detection of VPS34 and PIKfyve.

104   **(R)**HPLC detection of phosphoinositides in NOC18-treated HEK293 cells. Sample size

105   numbers are expressed in parenthesis, and pooled data is expressed as mean (SEM).

106   *p<0.05;**p<0.01;Scale bar:10μm. **Supplementary data: Figure 1-figure supplement 1**

NO downregulates phosphoinositides

107

108 We proceeded to supplement NOC18-treated cells with PI(3)P, and its isoforms PI(4)P or

109 PI(5)P, to ascertain specificity of PI(3)P effects. We observed that PI(3)P and PI(4)P resulted

110 in increased lysosomes with no further increase in lysosomes with NOC18(**Figure 2A,D**),

111 whereas PI(3)P treatment abolished NOC18-mediated inhibition of lysosomal

112 proteolysis(**Figure 2B,E**) and decrease in autolysosomes(**Figure 2C,F**). Our observations on

113 the attenuation of NOC18 effects on autolysosomes with PI(5)P supplementation(**Figure**

114 **2C,F**), is also consistent with earlier observations that PI(5)P can activate autophagy in

115 PI(3)P-depleted cells(*18*). Part of this phenomenon could be attributed to an increase in

116 lysosomes with PI(5)P supplementation(**Figure 2A,D**). On the other hand, PI(4)P did not

117 activate autophagy, contrary to previous observations(*18*), but supplementation of PI(4)P

118 suggested possible lysosomal proteolytic inhibition. Conversely, no further lysosomal

119 accumulation with NOC18 treatment in HEK 293 cells with siRNA-knockdown of

120 VPS34(**Figure 2-figure supplement 1 A**), nor was there any further decrease in lysosomal

121 proteolysis or autophagic impairment(**Figure 2-figure supplement 1 B-C**). Overall, our

122 observations suggest that NOC18-mediated reduction of PI(3)P levels via VPS34 inhibition

123 could account for NOC18-mediated lysosomal proteolytic and autophagic inhibition. As

124 PI(3)P is essential for PI(3,5)P$_2$ synthesis, we next tested whether VPS34 effects are mainly

125 via PI(3)P or its downstream metabolite PI(3,5)P$_2$. We proceeded to knock down ATG14,

126 another component of the VPS34-kinase complex, and supplemented the cells with either

127 PI(3)P or PI(3,5)P$_2$. First, we confirmed that ATG14 siRNA knockdown reduced intracellular

128 PI(3)P compartments, and supplementation of PI(3)P in ATG14 siRNA-knockdown cells

129 increased PI(3)P compartments (**Figure 2-figure supplement 1D**). Next, we found that

130 autophagic impairment by ATG14 was reversed with PI(3)P but not PI(3,5)P$_2$(**Figure 2-**

131 **figure supplement 1D**), whereas lysosomal accumulation by ATG14 was attenuated by

132   PI(3,5)P_2 but not PI(3)P (**Figure 2-figure supplement 1 E**), suggesting that the effects of

133   VPS34 on PI(3)P and PI(3,5)P_2 synergistically modulate lysosomal accumulation and

134   proteolysis, and autophagy. Finally we validated the knockdown efficacies of both siRNAs

135   (**Figure 2-figure supplement 1 F,G**): despite significant levels of hVPS34 persisted after

136   siRNA transfection, we still observed significant autophagic and lysosomal deficits in

137   hVPS34-siRNA transfected cells. Finally, no alterations in the Beclin1-VPS34-ATG14

138   kinase complex was observed, whereas mTOR interaction with VPS34 is enhanced with

139   NOC18(**Figure 2-figure supplement 1 H**), suggesting that the mTOR-VPS34 complex is

140   unique and does not interfere with Beclin1-VPS34-ATG14 complex interaction.

141

142   Next we supplemented NOC18-treated cells with PI(3,5)P_2 and observed that NOC18-

143   mediated lysosomal accumulation was markedly attenuated by PI(3,5)P_2 (**Figure 2G,J**),

144   while modest increases in lysosomal proteolysis (**Figure 2H,K**) and autophagy (**Figure 2I,L**)

145   were observed with PI(3,5)P_2 supplementation. Similarly, supplementation of PI(3,5)P_2 and

146   PI(3)P in rat cortical neurons reversed NO-mediated lysosomal accumulation (**Figure 2M,O**),

147   and proteolysis (**Figure 2N,P**) respectively. We then hypothesized that disruption of

148   PIKfyve-Fig4-Vac14 complex, an essential complex required for PI(3,5)P_2 synthesis, by NO

149   could mediate lysosomal impairment. We observed that Fig4-, PIKfyve-, and Vac14-siRNA

150   knockdown alone led to lysosomal accumulation, and no further lysosomal accumulation was

151   observed with NOC18 treatment(**Figure 2-figure supplement 1 I**). Paradoxically, we

152   observed attenuation of NOC18-mediated lysosomal proteolysis(**Figure 2-figure**

153   **supplement 1 J**) and autophagic impairment(**Figure 2-figure supplement 1 K**) in Fig4-,

154   PIKfyve- and Vac14-siRNA transfected cells. **Figure 2-figure supplement 1L** shows

155   knockdown efficacy of these siRNAs. Similarly, we found that YM201636, a PIKfyve

156   inhibitor, attenuated NOC18-mediated inhibition of autophagy (**Figure 2-figure supplement**

157   **1 M**) and lysosomal proteolysis(**Figure 2-figure supplement 1 N**), and lysosomal

158   accumulation (**Figure 2-figure supplement 1 O**). Taken together, our findings suggest that

159   PI(3)P deficiency from VPS34 inhibition mediates autophagosomal and lysosomal

160   proteolytic impairment, whereas PI(3,5)P$_2$ deficiency, contributed by PIKfyve and, to a

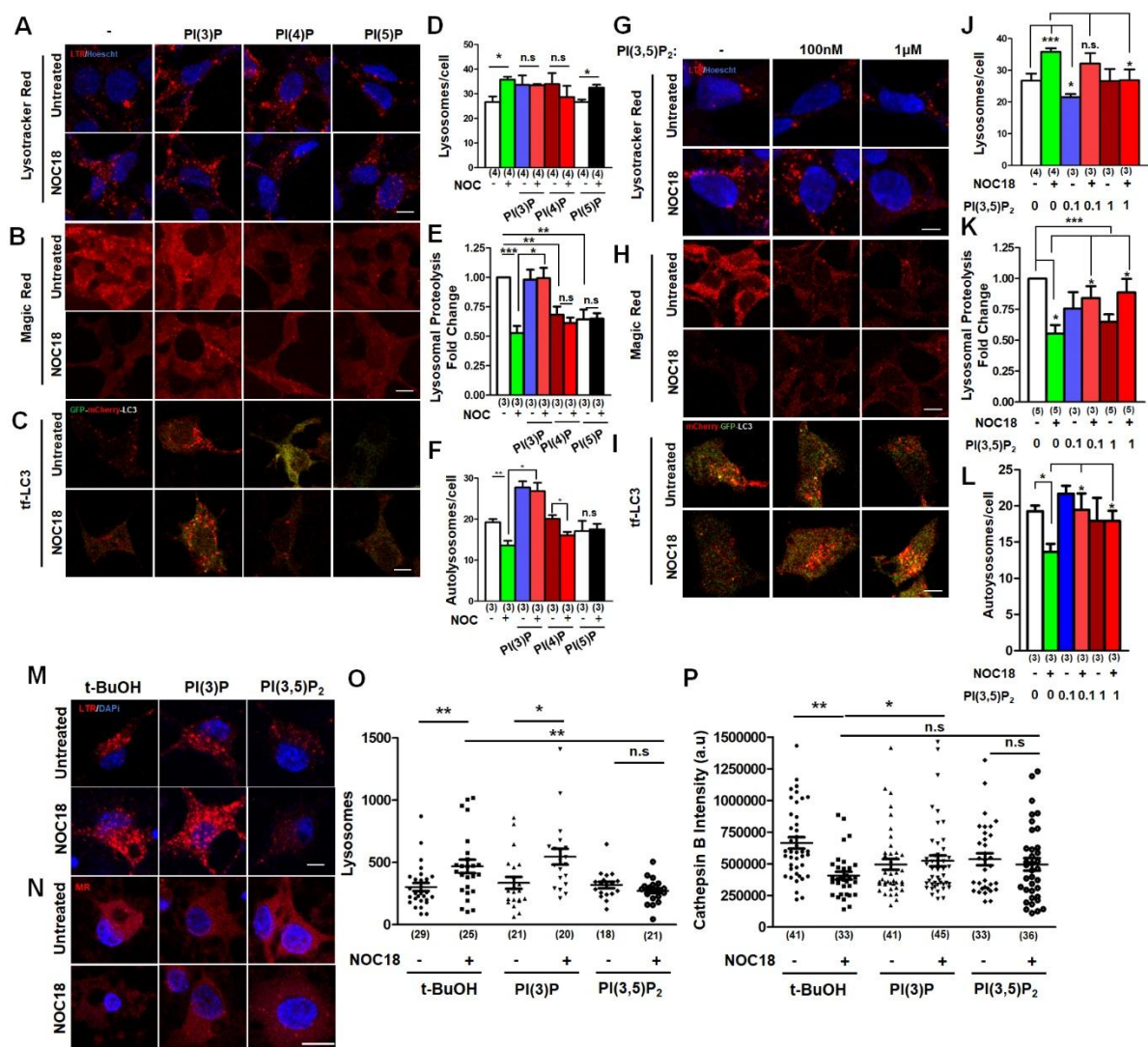161   smaller extent, VPS34 inhibition, mediates lysosomal accumulation by NOC18.

162   **Figure 2**

163
164

165 **Figure 2: PI(3)P and PI(3,5)P$_2$ supplementation reversed NO-mediated inhibition of**

166 **lysosomal proteolysis.** **(A)**Lysotracker Red and **(B)**Magic Red staining, and

167 **(C)**overexpression of mCherry-GFP-LC3 (tf-LC3) in HEK293 cells supplemented with

168 PI(3)P, PI(4)P or PI(5)P, and treated with NOC18, and their respective quantifications**(D-F)**.

169 **(G)**Lysotracker Red staining, **(H)**overexpression of tf-LC3 and **(I)**Magic Red staining in

170 HEK293 cells treated with PIKfyve inhibitor YM201636. **(J)**Lysotracker Red and **(K)**Magic

171 Red staining, and **(L)**overexpression of tf-LC3 in HEK293 cells treated with 100nM or 1μM

172 PI(3,5)P$_2$ and NOC18. **(M)** Lysotracker Red and **(N)** Magic Red staining of rat cortical

173 neurons treated with NOC18 in the presence of PI(3)P or PI(3,5)P$_2$, and **(O, P)** their

174 respective quantification. Sample size numbers are expressed in parenthesis, and pooled data

175 is expressed as mean (SEM). *$p<0.05$;**$p<0.01$;***$p<0.001$;Scale bar:10μm.

176 **Supplementary data: Figure 2-figure supplement 1**

177

mTOR S-nitrosylation is implicated in AD

178

179 We next asked how mTOR S-nitrosylation occurs? By overexpressing eNOS, iNOS and

180 nNOS, we observed that eNOS, but not iNOS or nNOS, recapitulated fully NOC18 effects on

181 lysosomal accumulation(**Figure 3A,D**), lysosomal proteolysis(**Figure 3B,E**), and autophagic

182 impairment(**Figure 3C,F**), although decreased lysosomal proteolytic activity was observed in

183 iNOS- and nNOS-transfected cells(**Figure 3B,E**). Correspondingly, these alterations in

184 lysosomal and autophagic activity were reversed by L-arginine analogue L-NAME(**Figure**

185 **3A-F**), suggesting that NO mediates these observed effects. Interestingly, we observed strong

186 and weak interaction of eNOS and iNOS with mTOR respectively, while only eNOS

187 overexpression recapitulated our earlier observations that mTOR has increased binding with

188 PIKfyve and VPS34(**Figure 3G-I**). Concomitantly, we observed increased S-nitrosylated

189 mTOR levels in eNOS- and iNOS-overexpressing cells(**Figure 3J,K**). To investigate the

190 physiological relevance of mTOR S-nitrosylation, we examined the APP/PS1 Alzheimer's

191 disease murine model and observed enhanced mTOR S-nitrosylation in APP/PS1 mouse

192 brains(**Figure 3L**). We proceeded to fractionate wild-type and age-matched APP/PS1 brains

193 and immunoprecipitated mTOR from cytosolic and lysosomal fractions. While no nNOS-

194 mTOR complexes in APP/PS1 lysosomal fractions were observed, there was an overall

195 decrease in lysosomal nNOS. Surprisingly, we observed nNOS-mTOR complexes in the

196 cytosolic fraction in the APP/PS1 brains(**Figure 3M**), which could suggest that other

197 cofactors specific in neuronal cell types could be involved in the complex formation. Next,

198 we found increased eNOS-mTOR complexes in the lysosomal fraction and decreased eNOS-

199 mTOR complexes in the cytosolic fraction of the APP/PS1 brains(**Figure 3M**). However, we

200 did not observe significant increase in iNOS-mTOR complexes in both cytosolic and

201 lysosomal fractions(**Figure 3M**). Lastly, we observed that mTOR-PIKfyve interaction occurs

202 in the lysosomal compartment, whereas mTOR-VPS34 interaction occurs in the cytosolic

203   fraction, suggesting that these two complexes are unique and are spatially separated, and are

204   both increased in APP/PS1 brains(**Figure 3M**). To investigate the physiological significance

205   of increased lysosomal mTOR-NOS in the APP/PS1 brains, we isolated lysosomes from

206   these mouse brains and observed increased NOS activity in APP/PS1 lysosomes, suggesting

207   that these complexes are functional(**Figure 3N**). Correspondingly, we observed lower

208   lysosomal β-glucosidase activity in APP/PS1 lysosomes(**Figure 3O**). As lysosomal arginine

209   is a potential substrate for lysosomal NOS, we hypothesize that S-nitrosylation of mTOR

210   could be an indicator for physiological sensing of lysosomal arginine. First, we observed that

211   lysosomal and autophagic activation by EBSS was attenuated with L-arginine

212   supplementation, but not L-NAME(**Figure 3-figure supplement 1 A-B**). Next, we observed

213   EBSS starvation decreased mTOR S-nitrosylation levels, and was rescued by L-arginine

214   supplementation but not L-NAME(**Figure 3P-Q**). In contrast, in rat brain-derived lysosomes,

215   pre-loading lysosomes with L-arginine, but not L-NAME, increased lysosomal NOS

216   independent of mTOR inhibition by Torin-1(**Figure 3R**). Lastly, lysosomes isolated from

217   ATG5-null mouse embryonic fibroblasts have increased NO activity, which suggest that

218   lysosomal NOS is dependent on cellular autophagic flux(**Figure 3S**). Taken together, our

219   data suggests that firstly, lysosomal arginine, a marker of amino acid nutrient status, mediates

220   mTOR S-nitrosylation under nutrient-replete conditions and acts as a physiological regulator

221   of lysosomal proteolysis and autophagy independent of mTORC1. Secondly, mTOR-eNOS

222   lysosomal localization could play a role in mediating mTOR S-nitrosylation and lysosomal

223   NO production from lysosomal L-arginine in AD.
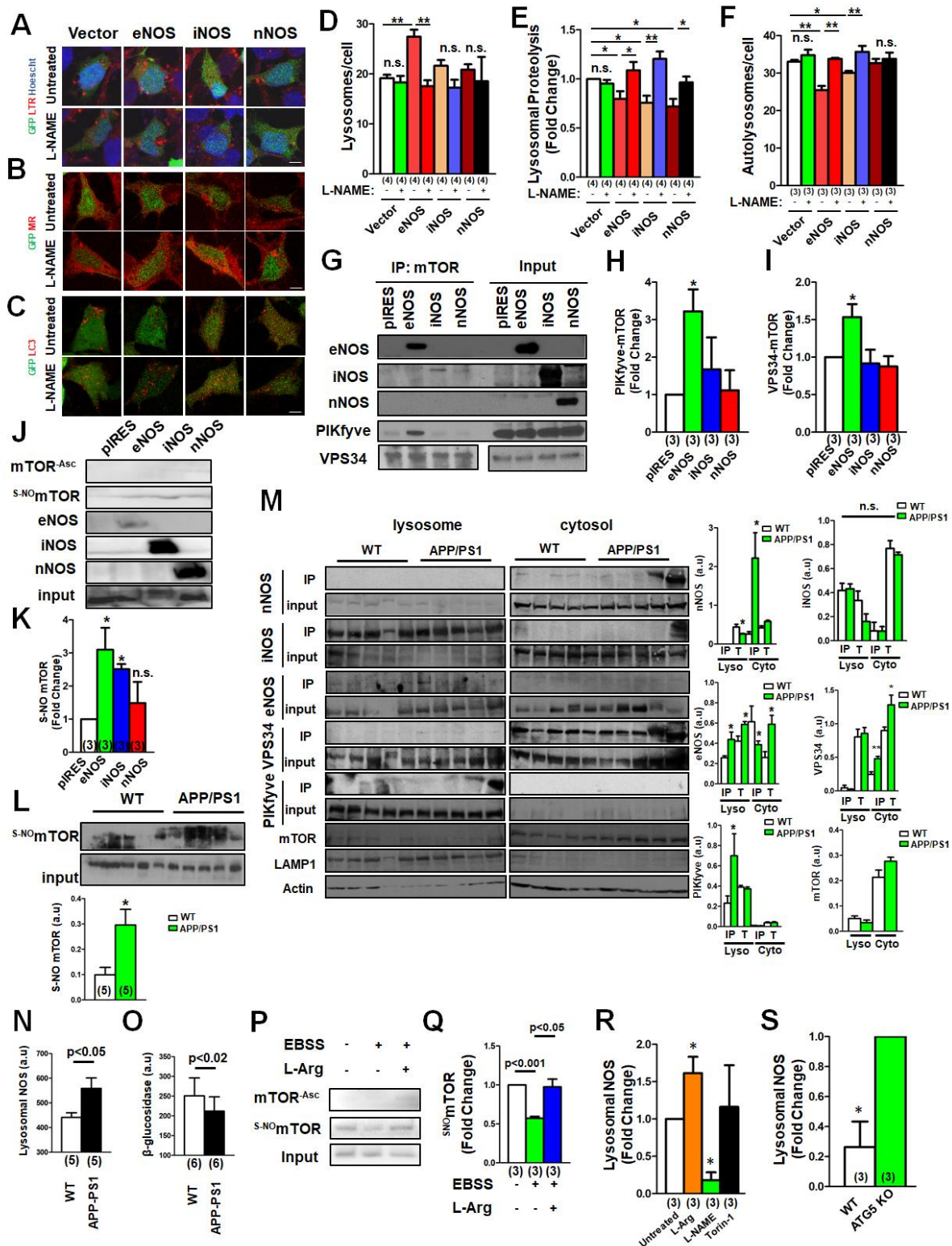
224

225   **Figure 3**

226

Figure 3: Lysosomal NOS mediates mTOR S-nitrosylation in AD. (A) Lysotracker Red

and **(B)**Magic Red staining of HEK293 transfected with GFP-pIRES (Vector), GFP-eNOS,

GFP-iNOS and GFP-nNOS, and treated with L-NAME. **(C)**Co-transfection of RFP-LC3 with

230   GFP-pIRES, GFP-eNOS, GFP-iNOS and GFP-nNOS, and **(D-F)**their respective puncta

231   quantification. **(G)**Immunoprecipitation of mTOR with overexpression of GFP-pIRES,

232   eNOS, iNOS and nNOS, and immunoblotting for eNOS, iNOS, nNOS, hVPS34 and PIKfyve

233   with **(H-I)** its respective densitometry analysis. **(J)**Resin-assisted capture (RAC) of

234   nitrosylated endogenous mTOR with GFP-pIRES, eNOS, iNOS and nNOS overexpression,

235   with **(K)**its respective densitometry analysis. **(L)**RAC performed on murine wild-type and

236   APP/PS1 whole brain lysate. **(M)**Cell fractionation of wild-type and APP/PS1 mice brains

237   with immunoprecipitation of mTOR and immunoblot for iNOS, nNOS, eNOS, PIKfyve,

238   VPS34, and mTOR, with loading controls actin and LAMP1. **(N)**Lysosomal NOS and

239   **(O)**proteolysis activity of lysosomes isolated from murine wild-type and APP/PS1 brains

240   ($p < 0.02$). **(P)**RAC performed on HEK293 cells subjected to EBSS-starvation and

241   supplemented with either L-arginine or L-NAME, and **(Q)**its respective densitometry

242   analysis. **(R)** NOS activity of rat brain-derived lysosomes pre-treated with L-arginine, L-

243   NAME or Torin-1, and **(S)** lysosomes derived from ATG5-knockout MEFs. Sample size

244   numbers are expressed in parenthesis, and pooled data is expressed as mean (SEM).

245   *$p < 0.05$;**$p < 0.01$;***$p < 0.001$;Scale bar:10μm. **Supplementary data: Figure 3-figure**

246   **supplement 1**

247

Cys423Ala-mTOR reverses AD pathology

To identify the site of S-nitrosylation on mTOR, we performed a mutant screen based on *in-silico* prediction(*19*) of cysteine residues that were most susceptible to S-nitrosylation, by performing site-directed mutagenesis (Cys>Ala) of 5 cysteine residues. Cys^{423}>Ala mTOR mutant(Cys^{423A}-mTOR) was the only mutant that reversed NOC18-mediated autophagic inhibition(**Figure 4A**), lysosomal accumulation(**Figure 4B**), and impaired lysosomal proteolysis(**Figure 4C**) without significant change in p70S6K phosphorylation, suggesting mTORC1-independent effects(**Figure 4-figure supplement 1 A-D**). Furthermore, *in silico* modelling suggests no significant protein structure changes with Cys423Ala mutation(**Figure 4-figure supplement 1 E,F**) that could affect its kinase activity. Correspondingly, we observed decreased S-nitrosylation levels with Cys^{423A}-mTOR(**Figure 4D**). We next observed that mTOR S-nitrosylation levels were elevated in 3 age-matched pairs of AD patient-derived fibroblasts:AG06869, AG07377, and AG08243, compared with healthy controls ND34791, AG04148, and GM01681 respectively(**Figure 4E,F**), and hypothesized that L-NAME or Cys^{423A}-mTOR overexpression could be novel therapeutic strategies in AD. We found that both L-NAME and Cys^{423A}-mTOR overexpression reversed lysosomal accumulation(**Figure 4G,H; Figure 4-figure supplement 1 G,H),** impaired lysosomal proteolysis(**Figure 4I,J; Figure 4-figure supplement 1 I,J**) and autophagy(**Figure 4K,L; Figure 4-figure supplement 1 K,L**) in AD fibroblasts, whereas no significant change in lysosomal proteolysis or autophagic activity was observed in the paired healthy controls. As a proof-of-concept, we next treated APP/PS1 mouse-derived hippocampi with L-NAME, and observed sustained late-LTP, typically absent in untreated APP/PS1 hippocampi(**Figure 4M,N**). Taken together, our data suggests that NOS-mediated mTOR S-nitrosylation is implicated in AD and could be a potential therapeutic target in reversing neurodegenerative processes stemming from autophagic and lysosomal failure.

273 **Figure 4**
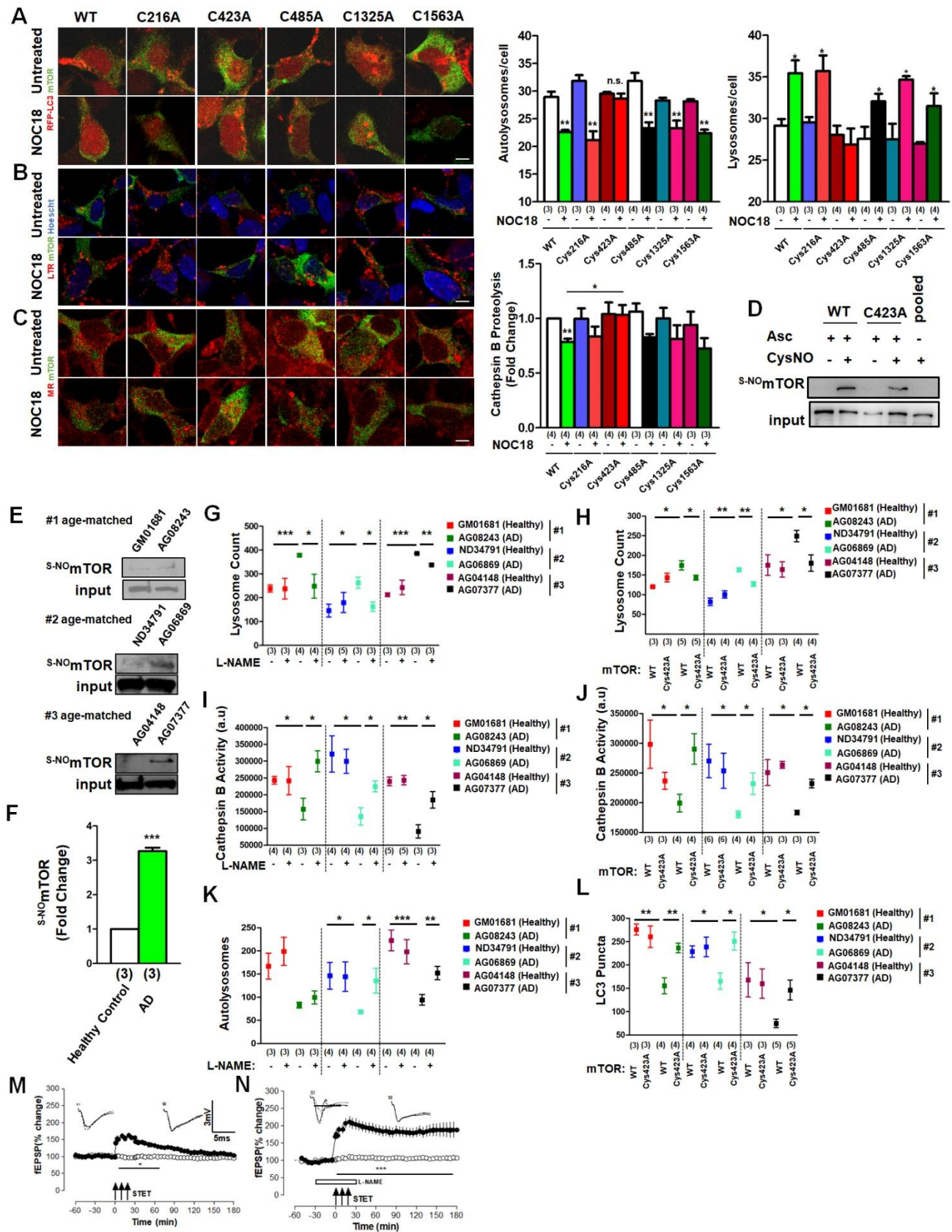
274

Figure 4: Cys423 S-nitrosylation of mTOR by lysosomal NOS is a therapeutic target in AD. (A) Overexpression of LC3, and **(B)**Lysotracker Red and **(C)**Magic Red staining of HEK293 cells transfected with mutant mTOR, and their corresponding quantification graphs. **(D)**RAC performed on wild-type mTOR and Cys^{423A}-mTOR, and **(E)**3 pairs of age-matched healthy controls(GM01681, ND34791, AG04148) and AD patient-derived fibroblasts(AG08243, AG06869, AG07377 respectively), with **(F)**its respective densitometry. **(G)**Lysosomal counts of healthy control and AD patient-derived fibroblasts subjected to L-NAME treatment and **(H)**Cys^{423A}-mTOR overexpression. (Lines are delineated for easy interpretation of a healthy control with the paired AD patient) **(I)**Lysosomal proteolysis activity of healthy control and AD patient-derived fibroblasts subjected to L-NAME treatment and **(J)**Cys^{423A}-mTOR overexpression. **(K)**Autolysosome counts of healthy control and AD patient-derived fibroblasts subjected to L-NAME treatment and **(L)**Cys^{423A}-mTOR overexpression. **(M)**L-LTP induced by STET in untreated APP/PS1 mice and **(N)**L-NAME pre-treatment. Filled circles represent S1 recording, while open circles represent stable control input S2. Analog traces represent fEPSP traces recorded from synaptic inputs S1 and S2 30-minutes before (dotted), 30-minutes (broken) and 3-hours (continuous) after tetanisation. Sample size numbers are expressed in parenthesis, and pooled data is expressed as mean (SEM). *p<0.05;**p<0.01;***p<0.001;Scale bar:10μm. **Supplementary data: Figure 4-figure supplement 1**

Discussion

mTOR has been classically defined as a kinase involved in regulation of the autophagosome-lysosomal pathway downstream of AMPK and PI3K-Akt signalling[20], whereby suppression of mTORC1 results in lysosomal and autophagic activation[21]. Here our study re-defines our understanding of the mTOR pathway with a kinase-independent, non-canonical mechanism of mTOR regulation via regulation of phosphoinositides. Previous studies reported that activation of lysosomal iNOS disrupts lysosomal function[14], while lysosomal arginine, a substrate of NOS, plays a critical role in lysosomal and autophagic regulation via mTORC1[5]. Our study reconciles these observations by proposing that lysosomal arginine serves as a marker of cellular nutrient status via mTOR nitrosylation. Finally, S-nitrosylation of mTOR is elevated in both Alzheimer's disease mice and human models, while antagonism of NOS activity or overexpression of Cys423Ala-mTOR mutant reversed lysosomal and autophagic deficits in Alzheimer's disease patient-derived fibroblasts, and LTP deficits in APP/PS1 hippocampi. In summary, our findings are in keeping with a phosphorylation-dominant mTOR signalling pathway in autophagic regulation which is sensitive to mTORC1 inhibitors, and provide an additional layer of complexity of mTOR regulation of autophagy and lysosomes (**Figure 5**). We propose that S-nitrosylation of mTOR is a potential therapeutic target for autophagic and lysosomal activation in aging and neurodegenerative diseases that minimizes systemic side effects of mTORC1 kinase inhibition precluding clinical utility.
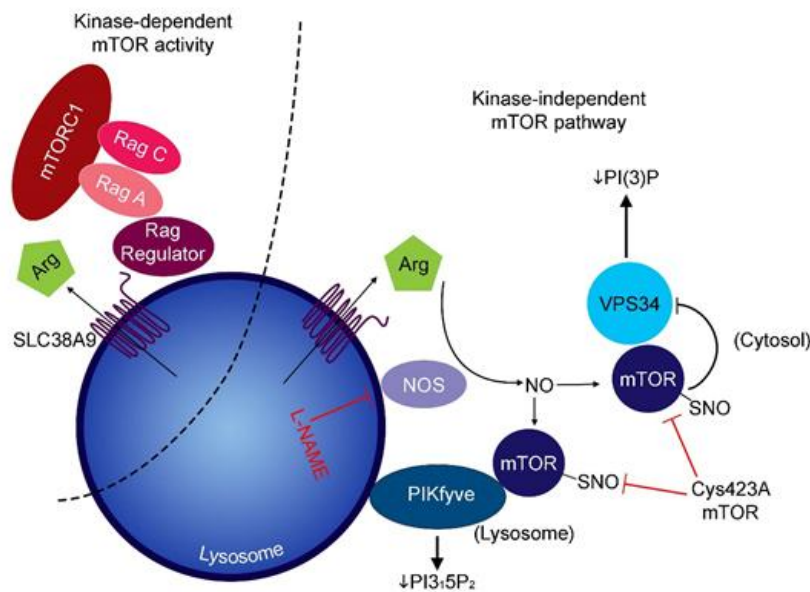
315 **Figure 5**

316

Figure 5: Kinase-independent effects of mTOR S-nitrosylation. Kinase-dependent

mTORC1 activity is associated with arginine-efflux lysosomal transporter SLC38A9

described in previous studies. Observations in this study suggest lysosomal arginine, under

nutrient-replete conditions, is transported out of the lysosome and converted to NO by

lysosomal nitric oxide synthases and consequently nitrosylating mTOR. S-nitrosylated

mTOR subsequently interacts with lysosomal PIKfyve and cytosolic VPS34 to decrease

PI(3,5)P$_2$ and PI(3)P respectively, thus downregulating lysosomal function and autophagy.

324

Materials and Methods

Cell culture Human embryonic kidney-293 (HEK293) cells were grown in DMEM

containing 10% FBS and 5% penicillin/streptomycin in 5% CO_2. To monitor the effect of NO

on autophagy, cells were treated with NO donor NOC-18 (4μM for 24 hr, Santa Cruz),

rapamycin (200nM, Sigma), Torin-1 (500nM or 1μM, Cayman Chemicals), wortmannin

(200nM, Cayman Chemicals), L-NAME (50μM, Sigma), L-arginine (0.4mM, Sigma),

YM201636 (1μM, Cayman Chemicals), PI(3)P-diC16 (1μM, Echelon), PI(4)P-diC16 (1μM,

332   Echelon), PI(5)P-diC16 (1μM, Echelon), and PI(3,5)P$_2$-diC8 (1μM, Echelon). HEK293 cells

333   were obtained from ATCC, and grown in DMEM containing 10% FBS and 5%

334   penicillin/streptomycin. ATG5 wild-type and knock-out mouse embryonic fibroblasts were

335   kind gifts from Dr Noboru Mizushima from Tokyo Medical and Dental University.

336   Transfection of plasmids or siRNA were performed at 70% and 50% confluency respectively.

337   siRNAs were transfected to achieve 0.5nM final concentration in media. Lipofectamine 2000

338   was used for transfection of HEK293 cells, and Lipofectamine 3000 for transfection of

339   patient-derived fibroblast cell lines as per manufacturer instructions for siRNAs and

340   plasmids.

341   **Animal Models:** All the experimental procedures were done in accordance with the

342   guidelines and protocols approved by the National University of Singapore (NUS)

343   Institutional Review Board and according to the guidelines of the Institutional Animal Care

344   & Use Committee (IACUC), NUS, Singapore. The AD mice model bears a chimeric

345   mouse/human APP with mutations linked to familial AD and a human PS1 carrying the exon-

346   9–deleted variant associated with familial AD under control of a prion promoter element

347   (APPSwe/PS1dE). 4 to 9 month old wild-type or APP/PS1 mice were used for biochemical

348   experiments, while age-matched male nontransgenic C57BL/6 mice were used as wild-type

349   controls for electrophysiological studies. A total of 10 APP/PS1 mice, and its corresponding

350   wild-type controls were used for the electrophysiological studies, while an additional 5

351   APP/PS1 mice and 5 wild-type control mice were used for biochemical characterization. Rat

352   whole brains were obtained from 6-week old wild-type rats, while cortical neurons from

353   wild-type rats were isolated in accordance to the protocol below.

354   **Patient-derived Fibroblasts:** Healthy age-matched controls (AG04148, ND034791,

355   GM01681) and idiopathic Alzheimer's Disease patients (AG07377, AG08243, AG07377)

356   were obtained from Coriell Institute, and overexpressed with GFP-mTOR or the Cys423Ala

357   mTOR mutant with Lipofectamine 3000.

358   **Rat Primary Neuron Culture** Primary rat cortical neurons were cultured using a modified

359   protocol as described previously(*22*). Briefly, rat embryonic day 16 (E16) to E18 cortical

360   neurons were cultured on glass coverslips coated with poly-D-lysine in Neurobasal medium

361   with B27 supplement (Invitrogen) containing 1% penicillin/streptomycin and 2mM

362   glutamine. 24h after plating, cultures were treated with 1μM cytarabine for 48h to remove

363   contaminating glia. Cells were used at 17 days *in vitro* (DIV 17) for all calcium imaging

364   experiments.

365   **Cell Fractionation:** Fresh rat or murine brain obtained from wild-type or APP-PS1, or SH-

366   SY5Y cells were equilibrated in lysosomal extraction buffer (135mM K, 45mM Cl, 90mM

367   gluconate, 30mM HEPES-NaOH, 30mM sucrose, pH 7.40) and dounced 40 times using a

368   homogenezier or syringed 40 times using a 27G needle respectively on ice. Cell lysates were

369   then subjected to an initial 8000g spin, followed by a 20000g spin. Lysosomal pellet is

370   collected at the end of the 20000g spin, while the cytosolic fraction is obtained from the

371   supernatant.

372   **Lysosomal nitric oxide synthase activity assay:** Lysosomes are incubated with 1mg/ml L-

373   arginine and in lysosomal extraction buffer for 3 hours, and NO metabolites are measured

374   using the diaminonaphthalene (DAN) assay. Briefly supernatant from the lysosome

375   suspension is added to a final concentration of 1mg/ml DAN dissolved in 0.1M HCl, and

376   incubated at 37°C for 15 minutes. The reaction is neutralized using equimolar volumes of

377   0.2M NaOH, and the reaction buffer is detected at 360 nm excitation, and 415 nm emission.

378   **Immunoblotting** The primary antibodies and their respective dilutions used in

379   immunoblotting are as followed, listed in alphabetical order: AKT (pan) (C67E7) (Cell

380   Signalling Technology (CST) #4691, 1:1000), ATG14 (CST #5504, 1:1000), β-actin (Abcam

381   ab8226, 1:10,000), β-tubulin (E7) (Developmental Studies Hybridoma Bank, 1:2000),

382   Beclin-1 (CST #3495, 1:1000), GFP (Roche Cat No 11814460001, 1:3000), mTOR (CST

383   #2972, 1:1000), Rictor (CST #2114, 1:500), Raptor (CST #2280, 1:500), p70/S6 kinase (CST

384   #2708, 1:1000), phospho-Akt^{T308} (CST #9275, 1:1000), phospho-Akt^{S473} (CST #4060,

385   1:1000), phospho-mTOR^{S2448} (CST #2974, 1:1000), phospho-p70/S6 kinase^{T389} (CST #9204,

386   1:1000), phospho-ULK1^{S555} (D1H4) (CST #5869, 1:1000), phospho-ULK1^{S757} (CST #14202,

387   1:1000), PIKfyve (Santa Cruz, sc-100408 1:1000), ULK1 (D8H5) (CST #8054, 1:1000), and

388   VPS34 (CST #4263, 1:1000).

389   **Immunoprecipitation** 1ug of mTOR, ATG14, Beclin-1, and VPS34 antibody was added into

390   cell lysates, and incubated overnight with Dynabeads. Immunoprecipitates were washed

391   extensively with cold PBS, and eluted with 6x SDS-loading buffer.

392   **Resin-Assisted Capture** Detection of S-nitrosylation of mTOR was done with resin-assisted

393   capture method as previously described(*23*).

394   **Plasmids** GFP-Rab7A^{WT} and Rab7A^{Q67L} mutant were gifts from Dr Gia Voeltz (Addgene

395   plasmid #61803)(*24*), GFP-LAMP1 was a gift from Dr Ron Vale (Addgene plasmid

396   #16290)(*25*), GFP-EEA1 was a gift from Dr Silvia Corvera (Addgene plasmid #42307)(*26*),

397   and RFP-LC3 was a gift from Dr Tamotsu Yoshimori (Addgene plasmid #21075)(*27*). GFP-

398   mTOR cysteine mutants – Cys216Ala, Cys423Ala, Cys485Ala, Cys1325Ala and

399   Cys1563Ala were generated by site-directed mutagenesis.

400   **Generation of GFP-TFEB SH-SY5Y stable cell line** GFP-TFEB expression construct and

401   blasticidin-resistant vector were purchased from the Addgene plasmid repository. SY5Y cells

402   were co-transfected with 1.0μg of GFP-TFEB construct together with 1.0μg of blasticidin-

403   resistant vector for 72h. Following transfection, positive cells co-expressing GFP-TFEB and

404   blasticidin-resistant vector were selected by killing with 10μg/ml blasticidin (Invitrogen) for

405   5-7 days. Co-transfected cells that survived blasticidin treatment were typsinized and re-

406   seeded to allow growth of single cell colonies under the influence of 10μg/ml blasticidin.

407   Positive clones were isolated, and allowed to grow and expand in the presence of 2μg/ml

408   blasticidin. The GFP-TFEB stable SY5Y cells were subsequently maintained in serum-

409   supplemented media supplemented with 2μg/ml blasticidin.

410   **Confocal Microscopy** Cells were stained with Lysotracker Red (1:2000, Thermoscientific)

411   for 1 hr, Cathepsin B substrate Magic Red (1:600, Immunochemistry) for 1 hr before fixing

412   in 2.5% PFA for 20 minutes. For analysis of autophagosomes or autolysosomes, cells were

413   transfected with RFP-LC3 or tandem-fluorescent LC3, and subjected to fixing in 2.5% PFA

414   for 20 minutes after treatment. Cells were extensively washed and stained with Hoescht

415   34222 (1:500, Immunochemistry). Confocal images were obtained from Zeiss LSM510

416   confocal microscope. Magic Red intensity was obtained using the AlexaFluor-594 excitation-

417   emission setting, with detection gain set between 750-850, and all images within each

418   biological replicate were taken with the same settings. Lysotracker Confocal images were

419   analysed using a semi-automated puncta counter using ImageJ for lysosomes and LC3

420   puncta, while densitometry-based analysis was performed for Magic Red fluorescent

421   intensity.

422   **Lysosomal enzyme activity measurement** Lysosomes extracted as described above were

423   resuspended in 1μM 4-methylumbelliferyl β-D-glucopyranoside (Sigma) for measurement of

424   β-glucosidase activity, or 1μM 4-methylumbelliferyl β-D-galactopyranoside (Sigma) for

425   measurement of β-galactosidase activity. To analyse effects of lysosomal calcium on

426   enzymatic activity, lysosomes were dialyzed with the MES standard buffers as described

427   above, and incubated with 20μM BAPTA-AM. Enzymatic reaction is quenched with 10mM

428 NaOH, and fluorescence intensities of excitation 360nm and emission of 450nm were

429 recorded.

430 **Hippocampal Slice Preparation and Electrophysiology.** Hippocampal slices were prepared

431 from 4-5 month old APP/PS1 mice. Mice were anaesthetized using CO_2 and then decapitated

432 immediately, after which the brains were quickly removed and cooled in 4-6 °C artificial

433 cerebrospinal fluid (ACSF). Hippocampi were dissected, and transverse hippocampal slices

434 (400 μm) were sectioned by using a manual tissue chopper. Slices were then immediately

435 incubated in an interface chamber (Scientific System Design) maintained at 32 °C for 2–3 h,

436 continuously perfused with oxygenated ACSF at a flow rate of 0.80 mL/min. The ACSF

437 contained the following (in mM): 124 NaCl, 4.9 KCl, 1.2 KH_2PO_4, 2.0 $MgSO_4$, 2.0 $CaCl_2$,

438 24.6 $NaHCO_3$, and 10 D-glucose, equilibrated with 95% O_2/5% CO_2 (32 L/h). In all

439 electrophysiological recordings, two-pathway experiments were performed, i.e., two

440 monopolar lacquer-coated, stainless-steel electrodes (5 MΩ; AM Systems) were positioned at

441 an adequate distance within the stratum radiatum of the CA1 region for stimulating two

442 independent synaptic inputs S1 and S2 of a neuronal population, thus evoking field EPSPs

443 (fEPSP) from Schaffer collateral/commissural-CA1 synapses. For recording the fEPSP,

444 (measured as its initial slope function), one electrode (5 MΩ; AM Systems) was placed in the

445 CA1 apical dendritic layer, and signals were amplified by a differential amplifier (model

446 1700; AM Systems). The signals were digitized by using a CED 1401 analog-to-digital

447 converter (Cambridge Electronic Design).

448 After the preincubation period, a synaptic input-output curve (afferent stimulation vs. fEPSP

449 slope) was generated. Test stimulation intensity was adjusted to elicit fEPSP slope of 40% of

450 the maximal EPSP response for synaptic inputs S1 and S2. For L-LTP induction, (a strong

451 tetanisation) STET protocol involving repeated high-frequency stimulation (three bursts of

452   100 pulses for 1 s (100 Hz) every 10 min) was performed. The pulse width was 0.2 ms per

453   phase and had double length in comparison with test pulse width. The slopes of the fEPSPs

454   were monitored online. Four 0.2-Hz biphasic constant-current pulses (0.1 ms per polarity)

455   were used for baseline recording at each time point.

456   The average values of the slope function of the field excitatory postsynaptic potential

457   (fEPSP) per time point were analyzed using Wilcoxon signed-rank test when compared

458   within the group or the Mann–Whitney U test when compared between groups.

459   **Phosphoinositide profiling** Phosphoinositide extraction was adapted from Kiefer *et al* (*12*)

460   and Nasuhoglu *et al (28)* as previously described. Chloroform (4 mL) was added to the cell

461   pellet and agitated for 10mins followed by addition of 2M HCl (2 mL), 2xPhosSTOP (2 mL),

462   2M NaCl (0.3 mL) and Methanol (4 mL) which contain 3mM BHT, 1mM NaF and

463   1xPhosSTOP. The mixture was vigorously vortexed and centrifuged. Lower organic phase

464   was separated and a second extraction with chloroform (4 mL) was conducted. The combined

465   organic phase was dried under a stream of nitrogen. Deacylation was then carried out by

466   addition of 4ml of $MeNH_2$ with the following composition water/methanol/n-butanol

467   (43:46:11) at $55^{o}C$ for 1 hr. The solvent was evaporated under reduced pressure and extracted

468   with water and an organic mixture of ethyl formate/n-butanol/petroleum ether (1/20/4). The

469   aqueous phase was concentrated and dry under vacuum. Freeze-dried samples were added

470   with 45 μL of water and 5 μL of 2-(4-hydroxyphenylazo)benzoic acid at 1000ppm as internal

471   standard . Samples were vortexed vigorously and centrifuged at 6000 rpm for 10mins, before

472   sonication was performed for 15mins. This was followed by vigorous vortexing and

473   centrifugation before injecting into the high-performance liquid chromatography (HPLC)

474   system. HPLC separation was performed on an Agilent 1100 coupled with LCQ Fleet Ion

475   trap Mass spectrometer. An Agilent Zorbax Eclipse Plus C18 (2.1x150mm) column was used

476   for the separation.

477   HPLC mobile phase A: water containing 5mM N,N-dimethylhexylamine and 4mM glacial

478   acetic acid. Mobile phase B: methanol containing 5mM N,N-dimethylhexylamine and 4mM

479   glacial acetic acid. Solvent gradient, 0 min 15% B, 60 min 50% B, 65 min 100% B and

480   remain 100% B for 15 min. The HPLC condition is modified from the report of Peter Küenzi

481   et al(*29*). Spectra was recorded from m/z of 200 to 600 in the negative mode. The

482   chromatogram obtained were smoothed and area under the respective phosphoinositide peaks

483   were integrated and normalized with PI.

In silico Protein Modelling

485   *In silico* modelling of the protein structures of wild-type mTOR and Cys423Ala-mTOR

486   mutant is done using the SWISS-MODEL open-access software as previously described(*30*).

Statistical Analysis

488   2-way Student's t-test was used for analysis of difference of means for lysosomal count,

489   autolysosomal and autophagosome counts, lysosomal proteolysis indices, lysosomal

490   perinuclear distribution, and Western blot densitometry. Paired Student's t-test was used for

491   analysis of lysosomal proteolytic activity in APP-PS1 and wild-type mice brains. All graphs

492   are represented as mean ± SEM, and the number of independent biological replicates or

493   sample size are indicated in parenthesis. A p-value of less than 0.05 is considered statistically

494   significant.

502   **Competing Interests:** The authors declare no competing interests.

503   **References**

504   1.   A. H. Tsang, Y. I. Lee, H. S. Ko, J. M. Savitt, O. Pletnikova, J. C. Troncoso, V. L.
505   Dawson, T. M. Dawson, K. K. Chung, S-nitrosylation of XIAP compromises neuronal
506   survival in Parkinson's disease. *Proc Natl Acad Sci U S A* **106**, 4900-4905 (2009).
507   2.   M. E. Conway, M. Harris, S-nitrosylation of the thioredoxin-like domains of protein
508   disulfide isomerase and its role in neurodegenerative conditions. *Front Chem* **3**, 27
509   (2015).
510   3.   A. Martinez-Ruiz, S. Lamas, S-nitrosylation: a potential new paradigm in signal
511   transduction. *Cardiovasc Res* **62**, 43-52 (2004).
512   4.   K. K. Chung, B. Thomas, X. Li, O. Pletnikova, J. C. Troncoso, L. Marsh, V. L.
513   Dawson, T. M. Dawson, S-nitrosylation of parkin regulates ubiquitination and
514   compromises parkin's protective function. *Science* **304**, 1328-1331 (2004).
515   5.   G. A. Wyant, M. Abu-Remaileh, R. L. Wolfson, W. W. Chen, E. Freinkman, L. V.
516   Danai, M. G. Vander Heiden, D. M. Sabatini, mTORC1 Activator SLC38A9 Is
517   Required to Efflux Essential Amino Acids from Lysosomes and Use Protein as a
518   Nutrient. *Cell* **171**, 642-654 e612 (2017).
519   6.   S. Wang, Z. Y. Tsun, R. L. Wolfson, K. Shen, G. A. Wyant, M. E. Plovanich, E. D.
520   Yuan, T. D. Jones, L. Chantranupong, W. Comb, T. Wang, L. Bar-Peled, R. Zoncu,
521   C. Straub, C. Kim, J. Park, B. L. Sabatini, D. M. Sabatini, Metabolism. Lysosomal
522   amino acid transporter SLC38A9 signals arginine sufficiency to mTORC1. *Science*
523   **347**, 188-194 (2015).
524   7.   S. Zahid, R. Khan, M. Oellerich, N. Ahmed, A. R. Asif, Differential S-nitrosylation of
525   proteins in Alzheimer's disease. *Neuroscience* **256**, 126-136 (2014).
526   8.   T. S. Wijasa, M. Sylvester, N. Brocke-Ahmadinejad, S. Schwartz, F. Santarelli, V.
527   Gieselmann, T. Klockgether, F. Brosseron, M. T. Heneka, Quantitative proteomics of
528   synaptosome S-nitrosylation in Alzheimer's disease. *J Neurochem* **152**, 710-726
529   (2020).
530   9.   P. Liu, M. S. Fleete, Y. Jing, N. D. Collie, M. A. Curtis, H. J. Waldvogel, R. L. Faull,
531   W. C. Abraham, H. Zhang, Altered arginine metabolism in Alzheimer's disease
532   brains. *Neurobiol Aging* **35**, 1992-2003 (2014).
533   10. D. H. Bergin, Y. Jing, B. G. Mockett, H. Zhang, W. C. Abraham, P. Liu, Altered
534   plasma arginine metabolome precedes behavioural and brain arginine metabolomic
535   profile changes in the APPswe/PS1DeltaE9 mouse model of Alzheimer's disease.
536   *Transl Psychiatry* **8**, 108 (2018).
537   11. E. Barbero-Camps, V. Roca-Agujetas, I. Bartolessis, C. de Dios, J. C. Fernandez-
538   Checa, M. Mari, A. Morales, T. Hartmann, A. Colell, Cholesterol impairs autophagy-
539   mediated clearance of amyloid beta while promoting its secretion. *Autophagy* **14**,
540   1129-1154 (2018).

12. Y. Wang, E. Mandelkow, Degradation of tau protein by autophagy and proteasomal pathways. *Biochem Soc Trans* **40**, 644-652 (2012).

13. D. S. Yang, P. Stavrides, P. S. Mohan, S. Kaushik, A. Kumar, M. Ohno, S. D. Schmidt, D. Wesson, U. Bandyopadhyay, Y. Jiang, M. Pawlik, C. M. Peterhoff, A. J. Yang, D. A. Wilson, P. St George-Hyslop, D. Westaway, P. M. Mathews, E. Levy, A. M. Cuervo, R. A. Nixon, Reversal of autophagy dysfunction in the TgCRND8 mouse model of Alzheimer's disease ameliorates amyloid pathologies and memory deficits. *Brain* **134**, 258-277 (2011).

14. Q. Qian, Z. Zhang, M. Li, K. Savage, D. Cheng, A. J. Rauckhorst, J. A. Ankrum, E. B. Taylor, W. X. Ding, Y. Xiao, H. J. Cao, L. Yang, Hepatic Lysosomal iNOS Activity Impairs Autophagy in Obesity. *Cell Mol Gastroenterol Hepatol* **8**, 95-110 (2019).

15. S. Sarkar, V. I. Korolchuk, M. Renna, S. Imarisio, A. Fleming, A. Williams, M. Garcia-Arencibia, C. Rose, S. Luo, B. R. Underwood, G. Kroemer, C. J. O'Kane, D. C. Rubinsztein, Complex inhibitory effects of nitric oxide on autophagy. *Mol Cell* **43**, 19-32 (2011).

16. H. X. Yuan, R. C. Russell, K. L. Guan, Regulation of PIK3C3/VPS34 complexes by MTOR in nutrient stress-induced autophagy. *Autophagy* **9**, 1983-1995 (2013).

17. C. H. Choy, G. Saffi, M. A. Gray, C. Wallace, R. M. Dayam, Z. A. Ou, G. Lenk, R. Puertollano, S. C. Watkins, R. J. Botelho, Lysosome enlargement during inhibition of the lipid kinase PIKfyve proceeds through lysosome coalescence. *J Cell Sci* **131**, (2018).

18. M. Vicinanza, V. I. Korolchuk, A. Ashkenazi, C. Puri, F. M. Menzies, J. H. Clarke, D. C. Rubinsztein, PI(5)P regulates autophagosome biogenesis. *Mol Cell* **57**, 219-234 (2015).

19. Y. Xue, Z. Liu, X. Gao, C. Jin, L. Wen, X. Yao, J. Ren, GPS-SNO: computational prediction of protein S-nitrosylation sites with a modified GPS algorithm. *PLoS One* **5**, e11290 (2010).

20. K. Kawauchi, T. Ogasawara, M. Yasuyama, K. Otsuka, O. Yamada, Regulation and importance of the PI3K/Akt/mTOR signaling pathway in hematologic malignancies. *Anticancer Agents Med Chem* **9**, 1024-1038 (2009).

21. R. Puertollano, mTOR and lysosome regulation. *F1000Prime Rep* **6**, 52 (2014).

22. C. P. Poore, J. R. Sundaram, T. K. Pareek, A. Fu, N. Amin, N. E. Mohamed, Y. L. Zheng, A. X. Goh, M. K. Lai, N. Y. Ip, H. C. Pant, S. Kesavapany, Cdk5-mediated phosphorylation of delta-catenin regulates its localization and GluR2-mediated synaptic activity. *J Neurosci* **30**, 8457-8467 (2010).

23. M. T. Forrester, J. W. Thompson, M. W. Foster, L. Nogueira, M. A. Moseley, J. S. Stamler, Proteomic analysis of S-nitrosylation and denitrosylation by resin-assisted capture. *Nat Biotechnol* **27**, 557-559 (2009).

24. A. A. Rowland, P. J. Chitwood, M. J. Phillips, G. K. Voeltz, ER contact sites define the position and timing of endosome fission. *Cell* **159**, 1027-1041 (2014).

25. A. A. Minin, A. V. Kulik, F. K. Gyoeva, Y. Li, G. Goshima, V. I. Gelfand, Regulation of mitochondria distribution by RhoA and formins. *J Cell Sci* **119**, 659-670 (2006).

26. D. C. Lawe, V. Patki, R. Heller-Harrison, D. Lambright, S. Corvera, The FYVE domain of early endosome antigen 1 is required for both phosphatidylinositol 3-phosphate and Rab5 binding. Critical role of this dual interaction for endosomal localization. *J Biol Chem* **275**, 3699-3705 (2000).

27. S. Kimura, T. Noda, T. Yoshimori, Dissection of the autophagosome maturation process by a novel reporter protein, tandem fluorescent-tagged LC3. *Autophagy* **3**, 452-460 (2007).

28. S. Kiefer, J. Rogger, A. Melone, A. C. Mertz, A. Koryakina, M. Hamburger, P. Kuenzi, Separation and detection of all phosphoinositide isomers by ESI-MS. *J Pharm Biomed Anal* **53**, 552-558 (2010).

29. C. Nasuhoglu, S. Feng, J. Mao, M. Yamamoto, H. L. Yin, S. Earnest, B. Barylko, J. P. Albanesi, D. W. Hilgemann, Nonradioactive analysis of phosphatidylinositides and other anionic phospholipids by anion-exchange high-performance liquid chromatography with suppressed conductivity detection. *Anal Biochem* **301**, 243-254 (2002).

30. A. Waterhouse, M. Bertoni, S. Bienert, G. Studer, G. Tauriello, R. Gumienny, F. T. Heer, T. A. P. de Beer, C. Rempfer, L. Bordoli, R. Lepore, T. Schwede, SWISS-MODEL: homology modelling of protein structures and complexes. *Nucleic Acids Res* **46**, W296-W303 (2018).